

Dendritic spine geometry can localize GTPase signaling in neurons

Samuel A. Ramirez^{a,b}, Sridhar Raghavachari^c, and Daniel J. Lew^b

^aProgram in Computational Biology and Bioinformatics and ^bDepartment of Pharmacology and Cancer Biology, Duke University Medical Center, Durham, NC 27710; ^cDepartment of Biology, University of Maryland, College Park, MD 20742

ABSTRACT Dendritic spines are the postsynaptic terminals of most excitatory synapses in the mammalian brain. Learning and memory are associated with long-lasting structural remodeling of dendritic spines through an actin-mediated process regulated by the Rho-family GTPases RhoA, Rac, and Cdc42. These GTPases undergo sustained activation after synaptic stimulation, but whereas Rho activity can spread from the stimulated spine, Cdc42 activity remains localized to the stimulated spine. Because Cdc42 itself diffuses rapidly in and out of the spine, the basis for the retention of Cdc42 activity in the stimulated spine long after synaptic stimulation has ceased is unclear. Here we model the spread of Cdc42 activation at dendritic spines by means of reaction-diffusion equations solved on spine-like geometries. Excitable behavior arising from positive feedback in Cdc42 activation leads to spreading waves of Cdc42 activity. However, because of the very narrow neck of the dendritic spine, wave propagation is halted through a phenomenon we term geometrical wave-pinning. We show that this can account for the localization of Cdc42 activity in the stimulated spine, and, of interest, retention is enhanced by high diffusivity of Cdc42. Our findings are broadly applicable to other instances of signaling in extreme geometries, including filopodia and primary cilia.

Monitoring Editor

Leah Edelstein-Keshet
University of British Columbia

Received: Jun 16, 2015

Revised: Aug 13, 2015

Accepted: Aug 25, 2015

INTRODUCTION

Our mental processes are the result of the electrical activity of complex networks of neurons. A majority of the connections between the principal nerve cells occur at dendritic spines, which are femtoliter-sized protrusions emanating from the dendrites. These structures are highly dynamic; they can be remodeled, created, and eliminated as a result of synaptic activity. Such experience-dependent plasticity has been associated with learning and memory, suggesting that spines are a substrate for the storage of information in the brain (Lamprecht and LeDoux, 2004; Kasai *et al.*, 2010).

This article was published online ahead of print in MBoC in Press (<http://www.molbiolcell.org/cgi/doi/10.1091/mbc.E15-06-0405>) on September 2, 2015.

Address correspondence to: Samuel A. Ramirez (samurami@gmail.com).

Abbreviations used: GAP, GTPase-activating protein; GEF, guanine nucleotide exchange factor; LTP, long-term potentiation.

© 2015 Ramirez *et al.* This article is distributed by The American Society for Cell Biology under license from the author(s). Two months after publication it is available to the public under an Attribution–Noncommercial–Share Alike 3.0 Unported Creative Commons License (<http://creativecommons.org/licenses/by-nc-sa/3.0>).

“ASCB®,” “The American Society for Cell Biology®,” and “Molecular Biology of the Cell®” are registered trademarks of The American Society for Cell Biology.

Spine remodeling is usually associated with changes in synaptic connectivity. For example, long-term potentiation (LTP), a persistent enhancement of synaptic strength after synaptic activity, often leads to a sustained increase in spine size (Matsuzaki *et al.*, 2004). LTP and the associated increase in spine size are specific to the activated synapse. Spine stimulation also results in longer-range effects on adjacent spines, such as a reduction of the threshold stimulus required to induce LTP (LTP priming; Harvey and Svoboda, 2007). Moreover, induction of LTP has been associated with the creation of new spines at adjacent sites in the dendrite (Maletic-Savatic *et al.*, 1999; De Roo *et al.*, 2008). Plasticity induced by single spine stimulation therefore takes place over space scales ranging from the single spine to a neighborhood in the dendrite. How such physiological changes are regulated is not well understood, but Rho-family GTPases, which are known to control polymerization of the actin cytoskeleton and synaptic plasticity (Luo, 2002), are strong candidates to regulate such events over different space scales (Yasuda and Murakoshi, 2011).

Murakoshi *et al.* (2011) used fluorescence lifetime imaging to measure the spatiotemporal activity of the Rho GTPases RhoA and

Cdc42 after the induction of LTP in single identified spines. Both GTPases increased their activity persistently at the spine upon stimulation, but whereas the activity of RhoA spread out to the dendrite and adjacent spines (over several micrometers), the activity of Cdc42 remained restricted to the stimulated spine (a submicrometer compartment) for ~15 min. The differences in spreading were not simply due to differences in GTPase diffusion, as active RhoA and Cdc42 both diffused out of the spine on time scales of 5 s. These findings suggest that physiological changes over different length scales induced after single-spine stimulation may be regulated by the spread of GTPase activities. For example, the sustained specific increase in spine size may be controlled by localized activation of Cdc42, whereas neighborhood heterosynaptic effects like LTP priming and new spine formation may be controlled by the spreading activation of RhoA. The basis for the observed differences in spatial spread of GTPase activities is not understood. Moreover, elucidating the mechanisms that limit Cdc42 activation to a submicrometer-sized compartment is essential for a better understanding of the molecular basis of the synapse specificity of LTP and memory in general.

Rho-family GTPase biochemistry has been extensively investigated (Etienne-Manneville and Hall, 2002). GTPases become activated upon exchanging bound GDP for GTP, stimulated by guanine nucleotide exchange factors (GEFs). Activated GTPases are mainly associated with the plasma membrane, where they regulate effector proteins that control actin assembly and function. Deactivation occurs due to hydrolysis of bound GTP to GDP, stimulated by GTPase-activating proteins (GAPs). GDP-bound GTPases relocate to the cytosol upon binding guanine nucleotide dissociation inhibitors. Regulation of the activity and intracellular localization of GAPs and GEFs is believed to determine the activity profiles of GTPases (Tolias *et al.*, 2011).

Cdc42 regulation is best understood in yeast, where the GTPase establishes polarized cortical domains that guide budding and mating. In this case, mathematical models have been crucial to understand how polarization arises as an emergent property of the interplay of reactions and diffusion (Goryachev and Pokhilko, 2008; Mori *et al.*, 2008; Howell *et al.*, 2009; Klunder *et al.*, 2013). Positive feedback between Cdc42 and its activating GEF results in the clustering of Cdc42 in a region of the membrane, forming a polarity patch. Furthermore, depletion of a cytoplasmic “substrate” of the auto-regulated activation, for example, inactive Cdc42 or a GEF-containing complex, is believed to limit the growth of the polarity patch. Mathematical models of polarization are usually posed as systems of partial differential equations describing the spatiotemporal evolution of the concentrations of chemical species. For example, Mori *et al.* (2008) proposed a model in which the positive feedback leads to bistability, that is, the potential for stable high-GTP-Cdc42 “on” or low-GTP-Cdc42 “off” states, depending on the history of the system. In this model, starting with the uniform “off” state, an initial local stimulation results in growth of a region with Cdc42 “on.” The transition from “off” to “on” spreads as a wave until depletion of the inactive pool of Cdc42 in the cytosol halts the spread. This “wave-pinning” process yields a polarized situation in which “on” and “off” states coexist in the same cell.

The observation that GTPases in dendritic spines remain activated for a period of time at least an order of magnitude longer than the initial stimulus (Murakoshi *et al.*, 2011) is consistent with the existence of positive feedback in GTPase activation, just as in the yeast Cdc42 system. Indeed, it has been proposed that the mammalian Cdc42 GEF, β -PIX, participates in such feedback via the Cdc42 effector, p21-activated kinase (Shin *et al.*, 2002). However, a key

requirement for polarization in the yeast models, namely the depletion of cytoplasmic factors, is not likely to hold in the dendritic spine. The dendritic shaft presumably acts as an effectively inexhaustible source of cytoplasmic substrates because of its much larger volume than that of the spine. Thus, even if the expected positive feedback could explain the persistence of Cdc42 activation during LTP, it is unclear why that activation would be limited to the stimulated spine rather than spread throughout the dendrite.

Here we computationally explore the consequences of enacting yeast-style Cdc42 biochemistry in the context of a neuronal geometry. We show that the geometrical characteristics of dendritic spines provide a novel potential mechanism for limiting the spatial spread of Cdc42 activity that can explain experimental observations. We also compare the predictions from the geometrical wave-pinning mechanism with a theoretical formulation that describes wave dynamics on curved surfaces.

RESULTS

Basis for prolonged confinement of Cdc42 activity within a dendritic spine

We first address the basis for prolonged confinement of Cdc42 activity in the spine that receives synaptic input. A conceptually simple way to explain this phenomenon is that a Cdc42-directed GEF is activated locally at the synapse (e.g., at the spine head). Assuming no feedback and uniform first-order deactivation of Cdc42, the spread of active Cdc42 to the dendrite once the system has reached steady state depends on diffusion and the rates of activation and deactivation (Berezhevskii *et al.*, 2010). Furthermore, the shape of the spine may also affect the level of Cdc42 activity at the dendrite. To simulate these effects, we modeled the spatiotemporal dynamics of Cdc42 at the spine by numerically solving the reaction-diffusion equation for the concentration of GTP-bound Cdc42 (a) on spine-like geometries:

$$\frac{\delta a}{\delta t} = D_a \Delta_{LB} a + f \quad (1)$$

where D_a is the diffusion coefficient of active Cdc42 on the membrane, Δ_{LB} is the Laplace–Beltrami operator, which is a generalization of the Laplace operator for curved surfaces, and f is the rate of change of a due to activation and deactivation of Cdc42. For the foregoing scenario, f is described by a localized constant rate of activation in the upper part of the spine and first-order deactivation rate ($a\delta$) everywhere. Active Cdc42 diffuses from the source of activation (Figure 1A), and for a given diffusion coefficient and spine geometry, the steady-state spread of active Cdc42 can be tuned by altering the deactivation rate constant δ (Figure 1B).

Thus, in principle, an appropriate combination of rate constants and diffusion coefficient can yield compartmentalized Cdc42 activity within a spine. However, the rapid deactivation necessary to prevent escape of active Cdc42 into the dendritic shaft would lead to rapid inactivation of Cdc42 within the spine once synaptic transmission ceased (Figure 1B, inset). Moreover, the spread of activity into the dendrite would depend on spine geometry. For example, we observe a considerable change in the spread of Cdc42 for different spine lengths (Figure 1C) and a modest variation for different spine radii (Figure 1D). Thus, in order to get similar behavior from spines of different shapes (Murakoshi *et al.*, 2011), one would have to tune parameters in a spine-specific manner. Overall, these features make this simple model unattractive as a way to explain confinement of Cdc42 activity in different-shaped spines for prolonged periods extending well beyond the initial synaptic stimulation.

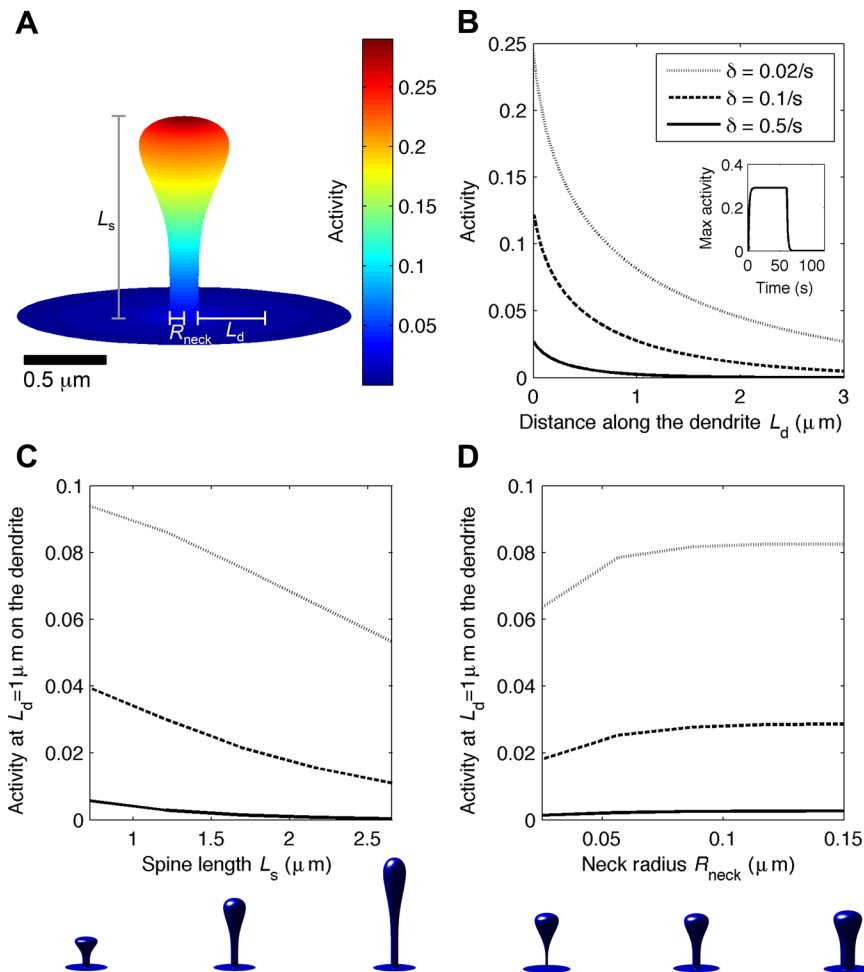


FIGURE 1: Simulations of the spread of active Cdc42 for the case of localized GEF activity at the top of the spine with uniform deactivation. (A) Profile of the concentration of GTP-Cdc42 at a spine connected to the dendrite. In the simulations, the dendrite membrane is represented by an annulus with outer radius $10\ \mu\text{m}$ connected to the spine. Here we show just a part of the dendrite membrane. The rate of activation is $1\ \text{s}^{-1}\ \mu\text{m}^{-2}$ over a symmetric area of $\sim 0.12\ \mu\text{m}^2$ at the top of the spine, and the diffusion coefficient is $0.25\ \mu\text{m}^2/\text{s}$. We show the results after $60\ \text{s}$ of stimulation with deactivation rate constant $\delta = 0.5/\text{s}$. (B) Radial profiles of the concentration of active Cdc42 on the dendrite for different δ . Inset, concentration of active Cdc42 at the top of the spine as a function of time ($\delta = 0.5/\text{s}$). The activation stimulus is turned on at $t = 0$ and off at $t = 60\ \text{s}$. (C) Concentration of active Cdc42 observed in the dendrite at a point $1\ \mu\text{m}$ away from the base of the spine for different spine lengths and (D) different spine radii, as depicted below the graphs.

Geometrical wave-pinning can yield long-lived but confined Cdc42 activation

As discussed in the *Introduction*, studies on Cdc42 in yeast and other cells suggest that Cdc42 regulators can provide positive feedback on Cdc42 activation (Kozubowski *et al.*, 2008; Johnson *et al.*, 2011). A simple model that recapitulates many aspects of such autoregulation was proposed by Mori *et al.* (2008). In this case, the reaction term f in Eq. 1 combines positive feedback on Cdc42 activation with first-order deactivation as

$$f(a, b) = b \left(k_0 + \frac{\gamma a^n}{K^n + a^n} \right) - \delta a \quad (2)$$

where a represents the concentration of active Cdc42 at the membrane and b represents the cytosolic concentration of inactive Cdc42. The first term on the right-hand side is a basal activation rate of Cdc42, and the second term describes an autocatalytic activation rate given by a Hill function with Hill coefficient n and saturation

parameter K . The third term is the rate of Cdc42 deactivation, where δ is a constant. The concentration of inactive Cdc42 is described by an equation analogous to Eq. 1 but defined in the cytosol. Because the total amount of Cdc42 ($a + b$) is conserved, the reaction term for b is $-f(a, b)$ at the boundary with the membrane.

This reaction scheme models the membrane as an excitable medium, where a localized stimulus can induce a switch from a low concentration of active Cdc42 ("off" state) to a high concentration of active Cdc42 ("on" state) in that region of the membrane. Activation of Cdc42 then propagates as a traveling wave front on the membrane. As the wave travels, active Cdc42 from the region that has already switched to the "on" state diffuses to the neighboring "off" region. This flow of active Cdc42 increases the concentration to a level at which the autocatalytic recruitment of Cdc42 from the cytosol triggers the transition to the "on" state (Mori *et al.*, 2008).

Mori *et al.* (2008) showed that for a cell with a fixed total amount of Cdc42, the spreading wave of cortical Cdc42 activity would lead to depletion of inactive Cdc42 in the cytosol, which in turn could halt the traveling wave of activation, a process termed "wave-pinning." The result is a final polarized configuration in which the "on" and "off" states coexist (Figure 2A). If inactive Cdc42 were not depleted, then the wave of activation would continue traveling until active Cdc42 completely covered the surface (Figure 2B). Because dendritic spines are very small compared with the whole dendrite, activation of Cdc42 in a single spine would not cause a significant reduction of inactive Cdc42 in the dendritic shaft. However, our simulations using this positive feedback scheme show that the activity of Cdc42 can remain localized within the spine even without any depletion of inactive

Cdc42 from the cytoplasm (Figure 2C). This form of wave-pinning arises purely from the geometry of the membrane.

To understand why spine geometry might constrain the spread of Cdc42 activity, consider what happens as the wave front of Cdc42 activation reaches the base of the spine. As it moves into the dendritic shaft, the wave front develops a circular shape that must expand for the wave to keep traveling (Figure 3, A and D). Because of the small radius of the spine neck ($0.025\text{--}0.15\ \mu\text{m}$; Harris and Stevens, 1989; Tonnesen *et al.*, 2014), the wave front at the spine base is highly curved, and active Cdc42 diffusing into the dendrite is rapidly dissipated into a larger area. Thus, the flow of active Cdc42 from the "on" region at the neck is no longer sufficient to activate the "off" region in the shaft. Increasing the radius of the spine neck results in a less curved wave front and hence a less dissipative flow of active Cdc42 (Figure 3, B and E). With a sufficiently large spine neck, the flow of active Cdc42 is able to trigger the switch from the "off" to the "on" state in the dendritic shaft, resulting in wave propagation

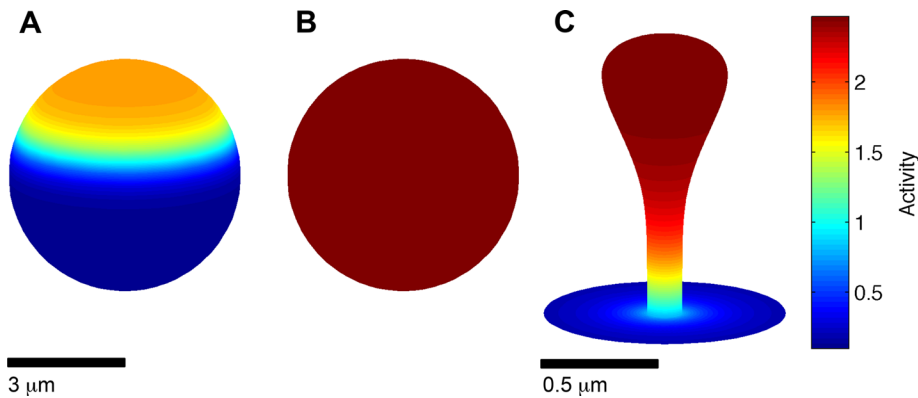


FIGURE 2: Spread of Cdc42 activity in a bistable model upon localized transient stimulation. (A) Depletion of inactive Cdc42 results in localization of active Cdc42 in one part of the membrane. (B) Without Cdc42 depletion, the entire membrane develops a high concentration of active Cdc42. (C) Membrane geometry can confine activation, resulting in localized sustained activity of Cdc42 at the spine without depletion of inactive GTPase.

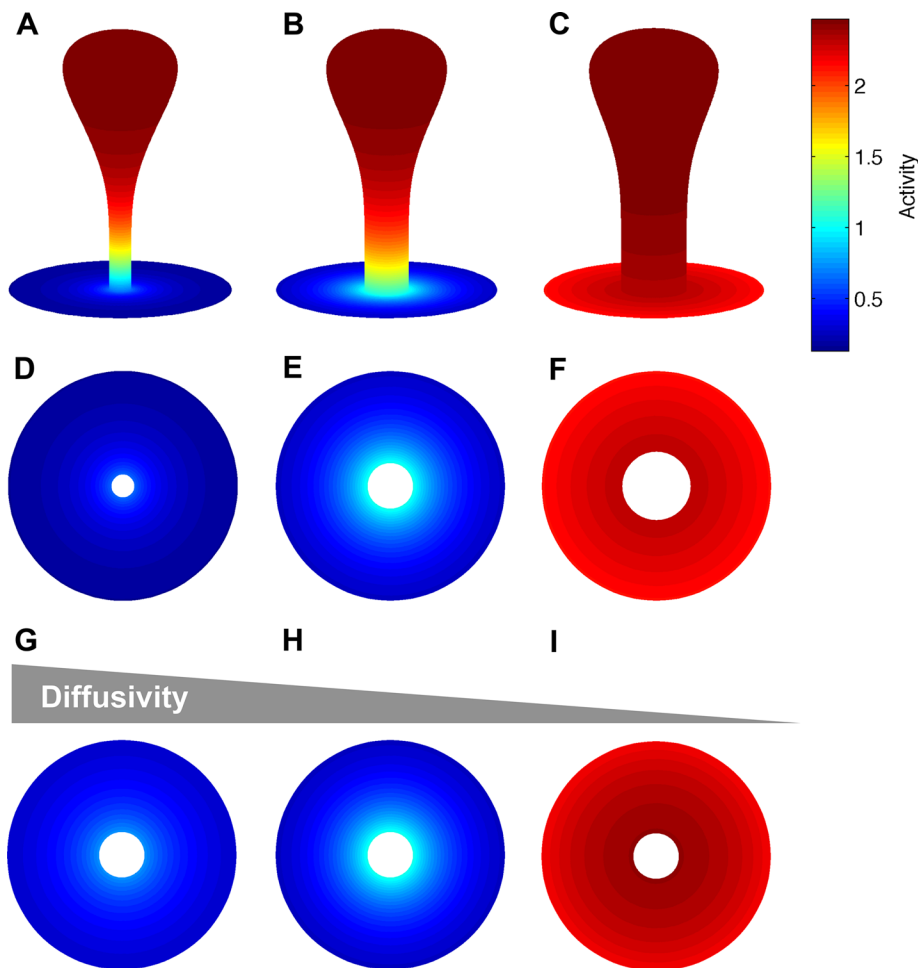


FIGURE 3: Narrow spine neck and high diffusivity promote localization of Cdc42 activity to the spine. Concentration of active Cdc42 at the membrane in a spine with neck radius (A) 0.05, (B) 0.1, and (C) 0.15 μm . In A–C, $D_a = 0.25 \mu\text{m}^2/\text{s}$. (D–F) Concentration of active Cdc42 at the annulus representing the membrane of the dendrite in proximity to the spine for A–C, respectively. (G–I) Concentration of active Cdc42 for neck radius 0.1 μm and diffusion coefficients (G) 0.8, (H) 0.25, and (I) 0.1 $\mu\text{m}^2/\text{s}$.

away from the spine (Figure 3, C and F). Note that high Cdc42 diffusivity at the membrane favors wave confinement by promoting the dissipation of activity at the dendrite close to the spine. Reduced diffusivity results in more accumulation of active Cdc42 close to the base of the spine and (with sufficiently slow diffusion) propagation of the wave of activation to the dendrite (Figure 3, G–I). Thus, counterintuitively, a faster-diffusing protein would be easier to confine by the geometrical wave-pinning mechanism.

Because a small neck radius promotes geometrical wave confinement, thinner necks can confine waves over a larger set of parameters. We quantify this effect in Figure 4, showing how wave confinement or propagation depends on the maximum autocatalytic Cdc42 activation rate γ (Figure 4, A and B) or the deactivation rate δ (Figure 4, C and D). In each case, we consider only parameter values that allow wave propagation within the spine. High γ or low δ enables Cdc42 diffusing from the “on” region to more effectively activate Cdc42 in the “off” region, promoting wave propagation to the dendrite shaft (Figure 4, A–D, white area). However, below a critical value of γ (or above a critical value δ), the wave can become confined by the geometry at the base of the spine (Figure 4, A–D, blue area). Smaller neck radii result in a larger parameter range yielding wave confinement. Similarly, increasing the diffusion coefficient makes it easier to confine the wave (Figure 4, B, D, and F).

The preceding analyses were restricted to the relatively narrow parameter regime in which the balance between Cdc42 activation and inactivation rates allows wave propagation in the spine. We can also vary both rates at the same time while maintaining this balance by writing the reaction term as

$$f(a,b) = k \left[b \left(0.05 + \frac{a^n}{K^n + a^n} \right) - a \right] \quad (3)$$

Here k determines the time scale of all reaction rates. k can be varied over a large range, yielding waves that propagate at different speeds. However, the qualitative behavior remains unchanged: decreasing the neck radius or increasing the diffusion coefficient enables wave confinement (Figure 4, E and F).

Comparison of simulations and theoretical predictions regarding signaling localization

The results from our simulations are in qualitative agreement with existing theory for propagation of waves with curved fronts on

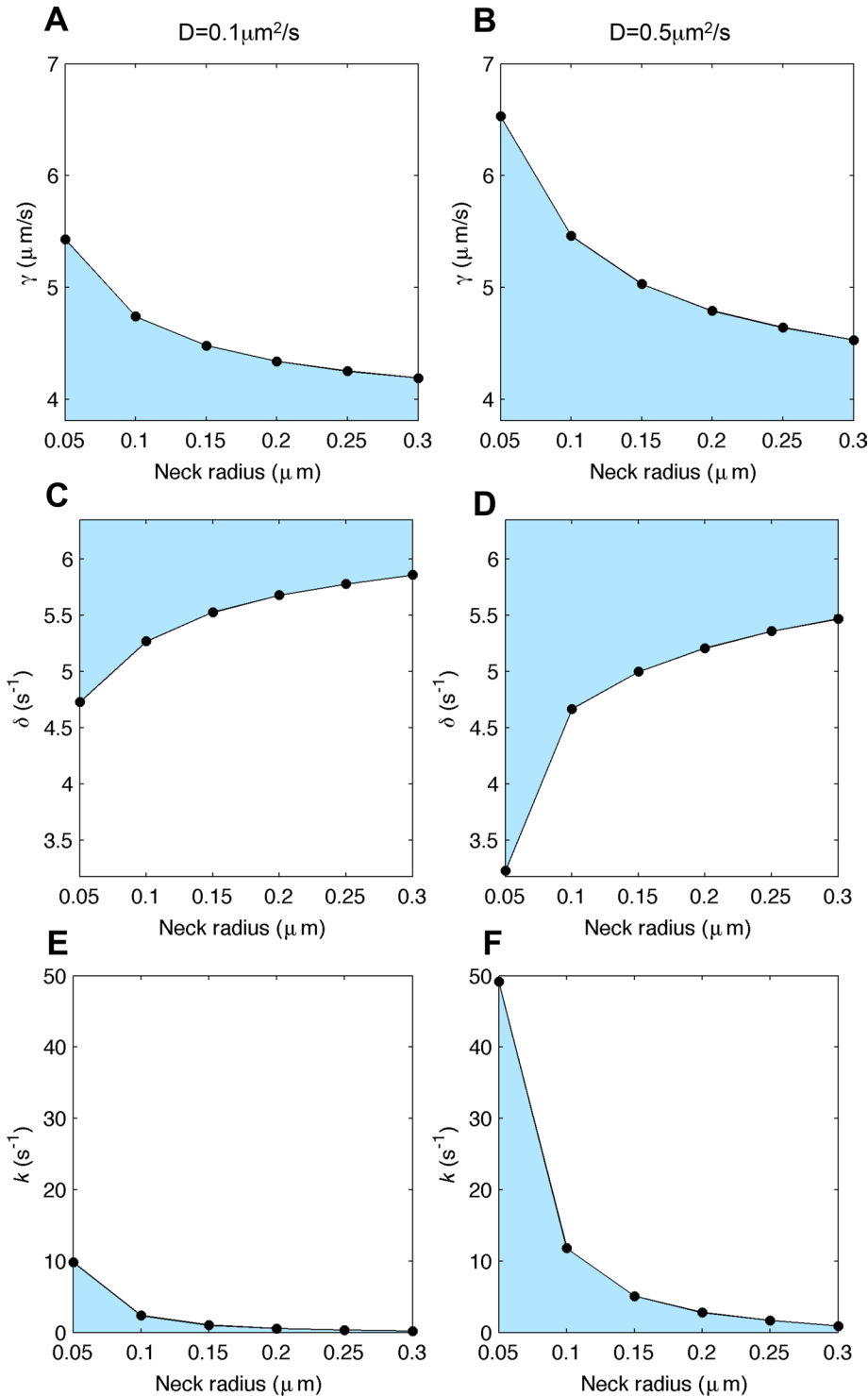


FIGURE 4: Phase diagrams showing the effect of spine neck radius and diffusivity on confinement of Cdc42 activation to the spine. White areas correspond to parameter regions where waves propagate to the dendrite, and blue areas indicate where the waves stay confined to the spine. (A, B) Varying γ , the maximum autocatalytic Cdc42 activation rate constant. (C, D) Varying δ , the deactivation rate; see Eq. 2. (E, F) Varying k , a parameter that determines the time scale of all the reaction rates; see Eq. 3. The diffusion coefficient is $0.1 \mu\text{m}^2/\text{s}$ for A, C, and E and $0.5 \mu\text{m}^2/\text{s}$ for B, D, and F.

excitable media. A wave front with positive curvature (e.g., an expanding circular wave) on a planar surface travels more slowly than a flat wave front. This occurs because as the curved wave travels,

respond to the boundary between the two regions in Figure 4E (also plotted in Figure 5A). According to the theory, k_c is such that

material (e.g., GTP-Cdc42) diffuses from a smaller region to a larger region, making it more difficult to trigger the switch to the "on" state in the region that is still in the "off" state. The higher the curvature, the greater is the dissipation and hence the slower is the travel. A quantitative approximation for this intuition is given by the eikonal equation

$$V = V_0 - KD \quad (4)$$

where V is the velocity of the wave, D is the diffusion coefficient on the surface, or D_a in this case, V_0 is the velocity of the wave when the front is flat, and K is the curvature of the wave front, or $1/R$ for a circular wave that is expanding (Zykov, 1980, 1987; Keener, 1986; Tyson and Keener, 1988). For a wave traveling on a curved surface, such as the spine membrane, K is replaced by the geodesic curvature, K_g (Davydov et al., 2000), which is the curvature of the projection of the wave front on the tangential plane. Along the spine neck, the membrane is approximately cylindrical, and the wave front traveling toward the dendrite has $K_g \approx 0$. After reaching the dendrite shaft, we assume that the surface is planar, and $K_g = K = 1/R$, where R is the radius of the circular wave front (Figure 5B). Therefore, near the intersection of the spine with the dendrite shaft,

$$V \approx V_0 \quad \text{at the neck} \quad (5)$$

$$V = V_0 - \frac{D}{R} \quad \text{at the dendrite}$$

Thus, as the wave front reaches the dendrite, the change in membrane geometry will induce a reduction in the velocity equal to D/R_{neck} (if $V_0 > D/R_{\text{neck}}$) or stop the wave altogether (if $V_0 \leq D/R_{\text{neck}}$). This theory agrees with the expectation that smaller R_{neck} and larger D would make it easier to stop the wave (geometrical wave-pinning), as illustrated in Figures 3 and 4. However, as discussed later, this theoretical approximation displays significant quantitative disagreement with the results of our numerical simulations.

To compare the predictions from the numerical solution of Eq. 1 and the eikonal equation, we use the reaction term in Eq. 3 and compute in both cases the maximum k (k_c) that results in wave confinement for different neck radii. The predicted values of k_c from simulations cor-

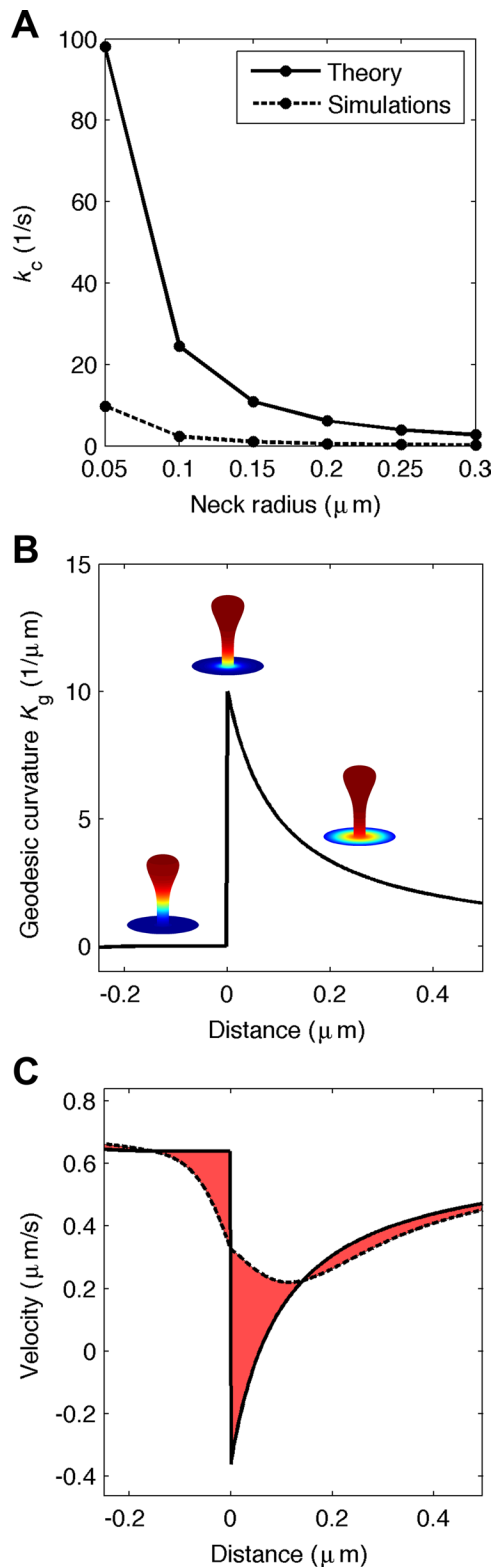


FIGURE 5: Comparison of simulations and theory for propagation of waves with curved fronts in a dendritic spine geometry. (A) Maximum k for confinement (k_c) predicted by simulations (dashed line) and theory (solid line). (B) Geodesic curvature (K_g) of a circular wave front as a function of geodesic distance from the base of the spine. Spine schemes show snapshots of a wave traveling into the dendrite. (C) Predicted wave velocity from simulations (dashed line) and theory (solid line). $k = 10/\text{s}$, $R_{\text{neck}} = 0.1 \mu\text{m}$, and $D_a = 0.1 \mu\text{m}^2/\text{s}$. The mismatch between the two is highlighted in red.

$$V_0(k_c) = \frac{D}{R_{\text{neck}}} \quad (6)$$

In this case, k_c can be estimated using the classical result, $V_0 \sim (kD)^{1/2}$ (see, e.g., Tyson and Keener, 1988) by determining the proportionality constant and replacing V_0 with D/R_{neck} according to Eq. 6. In Figure 5A, we see that Eq. 6 overestimates k_c , predicting confinement at values of k that result in spread of Cdc42 activation in simulations. Furthermore, the difference between theory and simulations becomes large when the neck radius is very small, as with dendritic spines. We note that reducing the space and time steps in our integration schemes did not affect the results significantly.

To better understand the mismatch between theory and simulation, we examined the behavior of waves that spread from the spine into the dendrite shaft (Figure 5B). Equation 4 predicts that the abrupt increase in geodesic curvature of a wave front at the junction of the spine neck with the dendrite (Figure 5B) would induce an equally abrupt drop in the wave velocity, which would then recover as the curvature decreases (Figure 5C, solid line). However, the simulations indicate a more gradual and less dramatic drop in wave velocity (Figure 5C, dashed line). The smaller effect of geodesic curvature in the simulations is correlated with the observation that it appears to be harder to stall a wave in simulations than predicted by Eq. 6 (Figure 5A).

An assumption in the derivation of Eq. 4 is that the wave profile does not change in time as the wave travels (Keener, 1986). However, we observe in our simulations that the wave profile can change considerably. For example, for the simulation in Figure 5C (dashed line), the maximum slope of the Cdc42 profile rose transiently as the wave transitioned from the neck of the spine into the dendrite (Figure 6A, dashed line). The transient increase in maximum slope results in faster flow of active Cdc42 from the "on" to the "off" region, thereby accelerating wave propagation and partly counteracting the slowing effect of curvature. This "buffering" by the change in wave profile therefore results in higher minimum velocities observed in the simulations than those predicted by the theory. The same effect may also explain the slower velocities predicted by simulations than theory when the wave is traveling at the dendrite (Figure 5C, right side of the plot). In this case, the maximum slope is reduced compared with the profile of a noncurved wave front (Figure 6A, solid line), therefore decelerating the wave.

To correct for the change in the wave profile resulting from the sudden change in curvature, we note that the flow of activated Cdc42, a , from the "on" region to the "off" region is proportional to the product of the maximum slope of the concentration profile and the diffusivity. Given that this flow mediates wave propagation, we might expect V_0 to be proportional to that product:

$$V_0 = \alpha D \max(\text{slope}) \quad (7)$$

Indeed, if we obtain a family of planar waves by varying k , we see a linear relation between V_0 and the maximum slope (Figure 6B). Extracting the proportionality constant α from this relation, we can then generate a revised prediction for curved geometries that incorporates the change in wave profile:

$$V = \alpha D \max(\text{slope}) - K_g D \quad (8)$$

This equation matches more accurately the velocity observed in simulations (Figure 6C) compared with the predictions of Eq. 4 (Figure 5C). The remaining mismatch occurs just around the base of the spine and is caused by the abrupt 90° angle at the base of the modeled spine. In simulations with a smooth transition between the spine and the dendritic shaft (Figure 7A), the change in

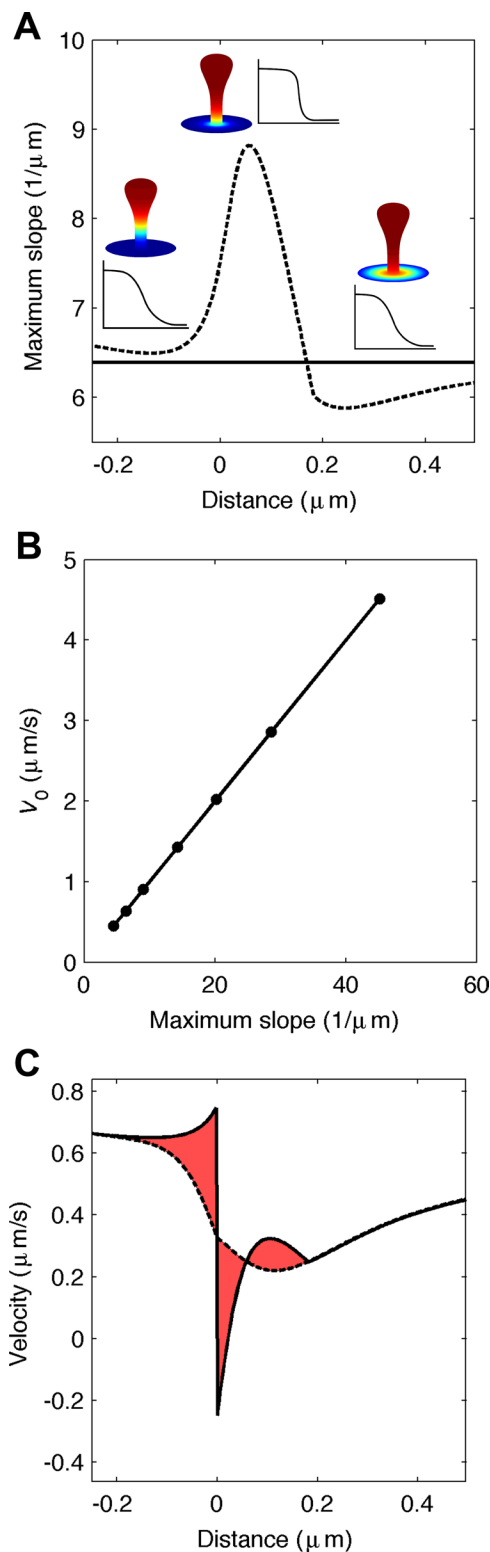


FIGURE 6: The mismatch between simulation and theory is due in part to a change in the profile of the wave as it traverses the base of the spine. (A) Maximum slope of the profile of Cdc42 activity as a wave with $k = 10/\text{s}$ travels on a spine with $R_{\text{neck}} = 0.1 \mu\text{m}$ (dashed line) and for a flat wave (solid line). $D_a = 0.1 \mu\text{m}^2/\text{s}$. We also show snapshots of the activity on the spine and cartoons of the profile of the activity vs. distance. (B) Flat wave velocity V_0 vs. the maximum slope of the profile of activity as k is varied. (C) Velocity from simulations (dashed line) and predicted by Eq. 8 (solid line) for the wave in A. The mismatch between simulations and Eq. 8 is visualized as a red area.

geodesic curvature is more gradual, and the mismatch between simulations and both Eqs. 4 (Figure 7B) and 8 (Figure 7C) is significantly reduced.

To enable wave spreading from the spine, the simulations discussed here used a low diffusion coefficient ($0.1 \mu\text{m}^2/\text{s}$) and a high value of k ($10/\text{s}$). For more physiological values ($D = 0.5 \mu\text{m}^2/\text{s}$, $k = 5/\text{s}$), confinement of active Cdc42 at the spine was still observed in a smoothed geometry (Figure 7D).

DISCUSSION

Geometrical wave-pinning as a way to confine signals to dendritic spines

It is widely accepted that the geometry of dendritic spines can partially isolate spine signaling from adjacent synapses by slowing diffusional escape of cytosolic molecules into the dendritic shaft (Gold and Bear, 1994; Hayashi and Majewska, 2005; Noguchi *et al.*, 2005; Tonnesen *et al.*, 2014). Recent theoretical simulations suggest that spine geometry may also restrict lateral diffusion of membrane receptors out of the spine (Kusters *et al.*, 2013). However, these confining attributes are insufficient to explain how Cdc42 activity remains localized to a spine for several minutes after glutamate stimulation despite diffusion time scales of a few seconds (Murakoshi *et al.*, 2011). Of note, the activity of other GTPases with similar diffusional characteristics can spread from the spine to the dendritic shaft (Harvey and Svoboda, 2007; Murakoshi *et al.*, 2011), suggesting that Cdc42 activity confinement arises from the specific mechanisms controlling that GTPase. This may have important physiological consequences, as Cdc42 is essential for LTP and is important for specific aspects of learning and memory and is distinct from other closely related GTPases such as Rac (Kim *et al.*, 2014). Because Cdc42 controls the actin-mediated remodeling of the spine during LTP, understanding long-term Cdc42 confinement is critical for explaining how LTP-associated spine remodeling is targeted specifically to the stimulated spine.

Here we propose a mechanism for confinement of Cdc42 activity that depends both on the geometry of the membrane and on the propagation of Cdc42 activity as a wave front. Wave-like spreading of activity can occur when a signaling pathway is excitable, as in many biological systems, including those of GTPases controlling actin (Hodgkin and Huxley, 1952; Tyson and Murray, 1989; Iglesias and Devreotes, 2012; Allard and Mogilner, 2013). In particular, Cdc42 activation is subject to positive feedback regulation (Johnson *et al.*, 2011), which can result in a bistable regulatory landscape that enables propagation of waves of Cdc42 activity (Mori *et al.*, 2008). We further demonstrate using simulations that the narrow neck of the spine can confine such waves of Cdc42 activity. This “geometrical wave-pinning” arises due to the high membrane curvature at the intersection between the spine and the dendritic shaft, which prevents the activity wave from spreading into the shaft while maintaining high Cdc42 activity within the spine.

In contrast to diffusional escape, which is enhanced by a high diffusion coefficient, for geometrical wave-pinning, a high diffusion coefficient enhances confinement of Cdc42 within the spine. This counterintuitive effect arises because more rapid diffusion of Cdc42 in a wave front with positive curvature allows more rapid dissipation of Cdc42 activity in the neighboring membrane, reducing or blocking wave propagation. Thus the activation of Cdc42 is easier to constrain within the spine if it diffuses rapidly.

Our results are broadly consistent with theoretical studies on how surface geometry can affect wave propagation, as expressed in the quantitative approximation known as the “eikonal equation” (Zykov, 1980, 1987; Keener, 1986; Davydov *et al.*, 2000). However,

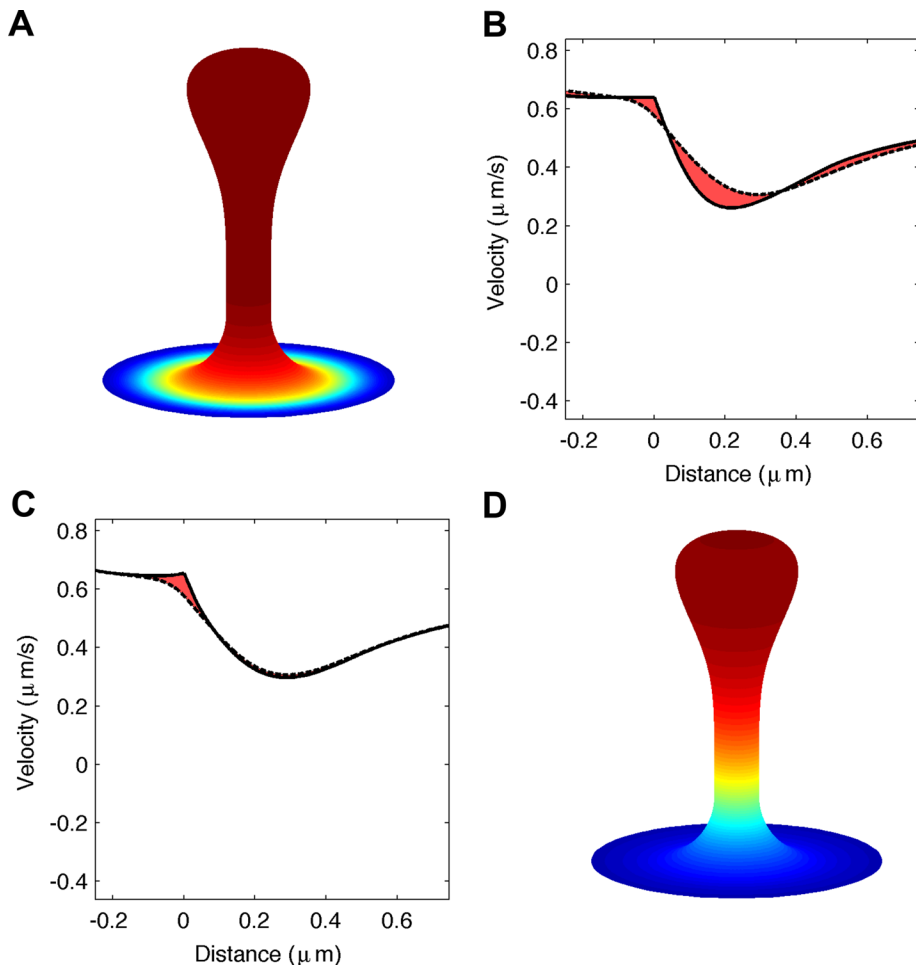


FIGURE 7: The mismatch between simulation and theory is reduced with a smooth transition at the base of the spine. (A) Smooth surface at the intersection between the spine and the dendritic shaft results in smaller mismatch between the velocity from simulations (dashed lines) and the predictions of both Eq. 4 (B) and Eq. 8 (C). $k = 10/s$, $R_{\text{neck}} = 0.1 \mu\text{m}$, and $D_a = 0.1 \mu\text{m}^2/s$. (D) Localization of Cdc42 activity can still occur in a smooth geometry, in this case, $k = 5/s$ and $D_a = 0.5 \mu\text{m}^2/s$.

this approximation overestimates the confinement capacity of a given spine. This is the case because in the extreme geometry of the spine, the profile of a traveling wave gets distorted and lessens the change in velocity induced by surface curvature.

Although the activity of Cdc42 localizes at dendritic spines upon stimulation, the activity of other GTPases, such as RhoA and Ras, spreads out to adjacent spines (Harvey and Svoboda, 2007; Murakoshi *et al.*, 2011). This spread may lead to heterosynaptic effects (Yasuda and Murakoshi, 2011). In the model that we present here, the activation and deactivation rates can determine whether GTPase activity remains confined to the spine or propagates to the dendritic shaft (Figure 4). Thus a similar regulatory architecture can result in drastically different signaling spread by tuning a single parameter. A possible scenario is that RhoA and Ras are regulated in a similar way as Cdc42, but faster activation rate and/or slower deactivation rate brings signaling dynamics into the spreading regime (e.g., white areas in Figure 4). Alternatively, it could be that unlike Cdc42, Rho and Ras GTPases may not be subject to positive feedback or may be subject to a different form of feedback that does not result in wave propagation. We also note that the data from Murakoshi *et al.* (2011) show a slow decrease in the activity of Cdc42 once it has been localized to the spine. This decrease may be due

to additional regulation on Cdc42 activity—for example, negative feedback stemming from mechanical tension (Houk *et al.*, 2012). Such regulation is beyond the scope of this work but could be included in an extension of the model that we present here.

Implications for other systems

Our study adds to several recent findings that emphasize the potential effects of cell geometry on signal transduction and polarization (Meyers *et al.*, 2006; Neves *et al.*, 2008; Maree *et al.*, 2012; Dawes and Iron, 2013; Kusters *et al.*, 2013; Rangamani *et al.*, 2013; Schmick and Bastiaens, 2014). Our particular focus has been on excitable signaling in the context of the extreme geometry of the dendritic spine, with its characteristically narrow neck. We note that other cellular protrusions, including filopodia, some bristles (Tilney *et al.*, 1995), and primary cilia (Michaud and Yoder, 2006), also have very narrow necks. Primary cilia are hubs for Hedgehog and other signaling pathways (Singla and Reiter, 2006; Goetz and Anderson, 2010). Filopodia may also play signaling roles (Mattila and Lappalainen, 2008), and bristles are mechanotransduction organs (Guild *et al.*, 2005). Thus there may be many scenarios in which cells exploit extreme geometries to confine or facilitate signaling.

One scenario of particular interest concerns spinogenesis, the process by which dendritic spines first form. As with spine remodeling, synaptic activity and signaling through Rho-family GTPases are believed to play a critical role in spinogenesis (Hotulainen *et al.*, 2009; Goh and Ahmed, 2012). However, there is controversy over whether

spines form from preexisting filopodia or directly from the dendritic shaft (Yuste and Bonhoeffer, 2004; Ethell and Pasquale, 2005; Ebrahimi and Okabe, 2014). One hypothesis is that short-lived filopodia search the space to establish the first connection with an incoming axon. On synaptic communication, the filopodium transforms into a spine in a process mediated by regulation of the actin cytoskeleton. If the initiating synaptic input were to occur at the dendritic shaft, it would take a strong signal to activate the GTPases (Figure 8A). This is because synaptic signaling in a very small patch would have the same large, positive curvature issues that we discussed with regard to wave propagation from the base of a very small spine neck. However, the sharp morphology at the tip of a filopodium and the high curvature at the base would facilitate the accumulation and retention of signaling GTPases at that site (Figure 8B), stimulating the remodeling of the filopodium into a new spine. The enhanced efficiency of GTPase activation conferred by the extreme geometry of the filopodium may therefore facilitate the formation of spines from these structures.

MATERIALS AND METHODS

Representation of the spine surface

We represent the shape of the spine with the surface of revolution of the parametric curve:

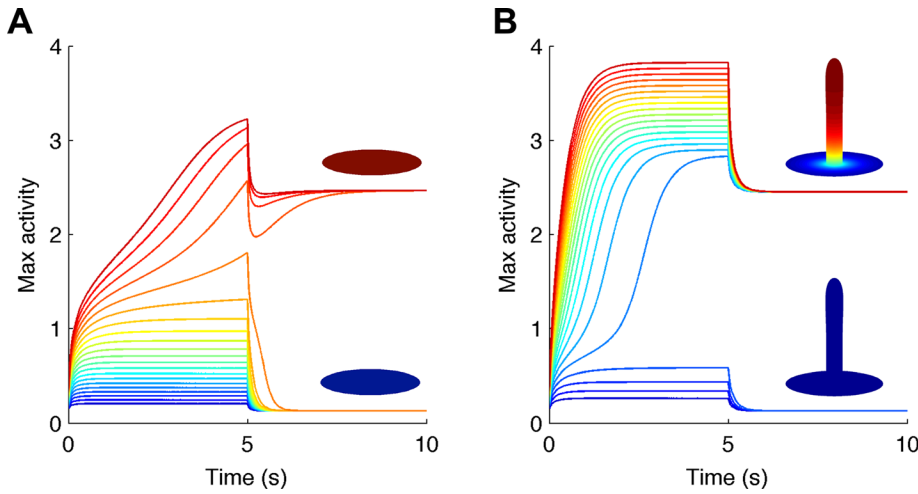


FIGURE 8: Filopodial geometry facilitates sustained GTPase activation by a weak synaptic input. Stimulatory pulses of GEF activity lasting 5 s over a symmetric area of $0.031 \mu\text{m}^2$ were applied to a flat surface representing the dendritic shaft (A) or to the tip of a filopodium connected to the shaft (B). Strength of the pulse is indicated by the color (blue \rightarrow red, strength varies between 1 and $11 \text{ s}^{-1} \mu\text{m}^{-2}$). GTPase behavior is assumed to display positive feedback according to Eq. 2, and maximum concentration of active GTPase is graphed as a function of time. The insets show characteristic profiles of the activity on the surfaces after removal of the stimulus. At the dendritic shaft, GTPase activity would decay rapidly once stimulation ceased unless the stimulus was very strong, in which case it would trigger a wave that would spread along the shaft. At filopodia, intermediate stimulus strengths would lead to sustained, localized GTPase activity, potentially leading to actin remodeling and spine formation.

$$r(z) = \left(\frac{C(Dz)^6(A^2 - (Dz)^2)}{A^4} + B^2 \right)^{1/2}$$

with $z \geq 0$. For most of the simulations, at $z = 0$, this surface intersects the dendritic shaft membrane, which is represented by an annulus on the plane xy with inner radius B and outer radius that varies depending on the figure. In Figure 7, the transition from the spine to the dendritic shaft is represented by the surface of revolution of a quarter of a circle with radius $R_{\text{trans}} = 0.3$. In all the simulations, $A = 1.2$ and $C = 0.3$. In this parametric representation B is the radius of the spine, which varies in the simulations, and D is also varied to obtain different spine lengths, $L_s = z_{\text{max}}$, which are estimated by solving $r(z) = 0$. Here r and z are interpreted as having units of micrometers.

Space and time discretization

Because of the angular symmetry of both the geometry and the initial conditions, the solution of Eq. 1 is one dimensional and is obtained using geodesic coordinates (see, e.g., Davydov *et al.*, 2000; Farauco, 2002). In that coordinate system, Eq. 1 takes the form

$$\frac{\partial a}{\partial t} = D_a \frac{\partial^2 a}{\partial l^2} + D_a K_g \frac{\partial a}{\partial l} + f \quad (\text{M.1})$$

where l is the position along a geodesic (meridian), which is calculated from

$$\frac{dl}{dz} = \left(1 + \left(\frac{dr}{dz} \right)^2 \right)^{1/2}$$

Here K_g is the geodesic curvature at position l , that is, the curvature of the projection of a curve of constant l on the tangential

plane. At the surface of revolution representing the spine,

$$K_g = \frac{1}{r} \frac{dr}{dz} \left(\frac{dl}{dz} \right)^{-1}$$

At the dendrite,

$$K_g = \frac{1}{r}$$

We used a second-order finite difference space discretization of Eq. M.1. The step size dl was $0.002 \mu\text{m}$, which ensured that further reduction of dl would improve the accuracy of the estimated quantities by $<3\%$. At the external edge of the annulus representing the dendrite, we used no-flux boundary conditions. The time evolution was carried out with the second-order backward differentiation formula BDF-2. dt was selected making sure that further reduction did not change the accuracy of the estimated quantities for the given dl .

Wave simulations

For simulations of wave propagation, the concentration is initially set uniformly as a_{low} , which is the lowest solution of $f(a) = 0$. Transient stimulation is simulated with a rate of activation k_{trans} over a symmetric region

$l < l_{\text{trans}}$. The duration and strength of stimulation are enough to start a wave at the top of the spine that travels along the surface. In all simulations, the Hill coefficient $n = 3$. The concentration units are normalized such that $K = 1 \mu\text{m}^{-2}$. For all wave simulations except in Figure 2A, $b = 2.5 \mu\text{m}^{-3}$. In Figures 2, 3, 4, and 8 (unless otherwise stated), $\delta = 5 \text{ s}^{-1}$, $\gamma = 5 \mu\text{m/s}$, and $k_0 = 0.25 \mu\text{m}^2/\text{s}$. In Figures 2 and 8, $D_a = 0.25 \mu\text{m}^2/\text{s}$. This value for the diffusion coefficient, together with other values used here ($0.1\text{--}0.8 \mu\text{m}^2/\text{s}$), is consistent with experimental estimates of the diffusion coefficients of small GTPases in mammalian cells, which are $\sim 0.5 \mu\text{m}^2/\text{s}$ (Lommerse *et al.*, 2004; Murakoshi *et al.*, 2004; Yasuda and Murakoshi, 2011; Das *et al.*, 2015).

For Figure 2A, we consider the time evolution of the concentration of inactive Cdc42 (b) assuming that b is well mixed in the cytosol. In this case, the change in b is computed from the mass conservation relation:

$$\int_S a dS + bv = \text{constant}$$

where S is the surface and v is the volume of the sphere.

Phase diagrams

To compute the boundary of the phase diagrams in Figure 4, we ran simulations of waves that escape to the dendritic shaft and varied the parameter of interest (e.g., γ in Figure 4A) for a given neck radius until the wave remained localized to the spine. As we varied the parameter by decreasing it (γ , k) or increasing it (δ) by a small amount ϵ , we measured the time T_{trv} for the wave to travel from a position $l_{\text{ini}} = 0.5 \mu\text{m}$ on the spine from the base to a position $l_{\text{final}} = 0.5 \mu\text{m}$ on the dendrite from the base of the spine. The criterion to determine that a wave was localized at the spine was that it did not reach the position l_{final} after $4T_{\text{trv}}$ from the previous iteration. Figure 9 shows a plot of $1/T_{\text{trv}}$ as we vary k , to illustrate the iteration process.

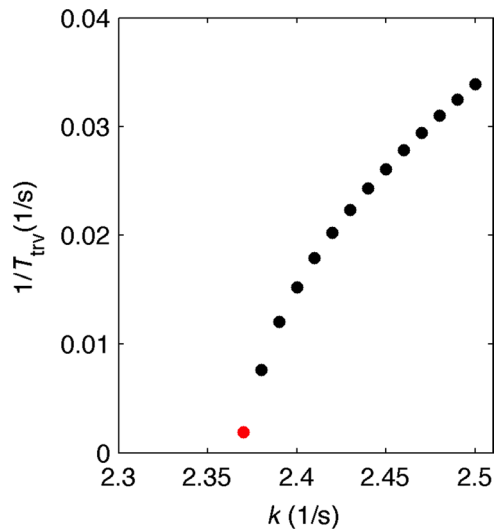


FIGURE 9: Iteration process to determine a critical parameter where a wave of activity no longer escapes to the dendritic shaft. As we decrease k , $1/T_{trv}$ approaches zero. The red point is the estimated critical k , which is subject to an error ϵ . $R_{neck} = 0.1 \mu\text{m}$ and $D_a = 0.1 \mu\text{m}^2/\text{s}$.

The range of parameters in Figure 4 is such that a one-dimensional system allows for wave propagation.

To estimate the position of the wave front in Figures 4–6, we defined that position as the location where the concentration of a has the value of the intermediate solution of $f(a) = 0$ (i.e., the threshold a concentration for switching between low- and high-activity states in a well-mixed system).

ACKNOWLEDGMENTS

We thank Nathan Hedrick, Scott Soderling, Tim Elston, the members of the Elston Lab, Patrick Charbonneau, and Tom Beale for stimulating discussion and comments on the manuscript. This work was supported by National Institutes of Health/National Institute of Mental Health Grant MH96376 to S.R. and National Institutes of Health/National Institute of General Medical Sciences Grant GM62300 to D.J.L.

REFERENCES

Allard J, Mogilner A (2013). Traveling waves in actin dynamics and cell motility. *Curr Opin Cell Biol* 25, 107–115.

Berezhtskovskii AM, Sample C, Shvartsman SY (2010). How long does it take to establish a morphogen gradient? *Biophys J* 99, L59–L61.

Das S, Yin T, Yang Q, Zhang J, Wu Y, Yu J (2015). Single-molecule tracking of small GTPase Rac1 uncovers spatial regulation of membrane translocation and mechanism for polarized signaling. *Proc Natl Acad Sci USA* 112, E267–E76.

Davydov VA, Morozov VG, Davydov NV (2000). Ring-shaped autowaves on curved surfaces. *Phys Lett A* 267, 326–330.

Dawes AT, Iron D (2013). Cortical geometry may influence placement of interface between par protein domains in early *Caenorhabditis elegans* embryos. *J Theor Biol* 333, 27–37.

De Roo M, Klausner P, Muller D (2008). LTP promotes a selective long-term stabilization and clustering of dendritic spines. *PLoS Biol* 6, e219.

Ebrahimi S, Okabe S (2014). Structural dynamics of dendritic spines: molecular composition, geometry and functional regulation. *Biochim Biophys Acta* 1838, 2391–2398.

Ethell IM, Pasquale EB (2005). Molecular mechanisms of dendritic spine development and remodeling. *Prog Neurobiol* 75, 161–205.

Etienne-Manneville S, Hall A (2002). Rho GTPases in cell biology. *Nature* 420, 629–635.

Farauo J (2002). Diffusion equation on curved surfaces. I. Theory and application to biological membranes. *J Chem Phys* 116, 5831–5841.

Goetz SC, Anderson KV (2010). The primary cilium: a signalling centre during vertebrate development. *Nat Rev Genet* 11, 331–344.

Goh WI, Ahmed S (2012). mDia1-3 in mammalian filopodia. *Commun Integr Biol* 5, 340–344.

Gold JI, Bear MF (1994). A model of dendritic spine Ca^{2+} concentration exploring possible bases for a sliding synaptic modification threshold. *Proc Natl Acad Sci USA* 91, 3941–3945.

Goryachev AB, Pokhilko AV (2008). Dynamics of Cdc42 network embodies a Turing-type mechanism of yeast cell polarity. *FEBS Lett* 582, 1437–1443.

Guild GM, Connelly PS, Ruggiero L, Vranich KA, Tilney LG (2005). Actin filament bundles in *Drosophila* wing hairs: hairs and bristles use different strategies for assembly. *Mol Biol Cell* 16, 3620–3631.

Harris KM, Stevens JK (1989). Dendritic spines of CA 1 pyramidal cells in the rat hippocampus: Serial electron microscopy with reference to their biophysical characteristics. *J Neurosci* 9, 2982–2997.

Harvey CD, Svoboda K (2007). Locally dynamic synaptic learning rules in pyramidal neuron dendrites. *Nature* 450, 1195–1200.

Hayashi Y, Majewska AK (2005). Dendritic spine geometry: functional implication and regulation. *Neuron* 46, 529–532.

Hodgkin AL, Huxley AF (1952). A quantitative description of membrane current and its application to conduction and excitation in nerve. *J Physiol* 117, 500–544.

Hotulainen P, Llano O, Smirnov S, Tanhuanpaa K, Faix J, Rivera C, Lappalainen P (2009). Defining mechanisms of actin polymerization and depolymerization during dendritic spine morphogenesis. *J Cell Biol* 185, 323–339.

Houk AR, Jilkine A, Mejean CO, Boltyanskiy R, Dufresne ER, Angenent SB, Altschuler SJ, Wu LF, Weiner OD (2012). Membrane tension maintains cell polarity by confining signals to the leading edge during neutrophil migration. *Cell* 148, 175–188.

Howell AS, Savage NS, Johnson SA, Bose I, Wagner AW, Zyla TR, Nijhout HF, Reed MC, Goryachev AB, Lew DJ (2009). Singularity in polarization: rewiring yeast cells to make two buds. *Cell* 139, 731–743.

Iglesias PA, Devreotes PN (2012). Biased excitable networks: how cells direct motion in response to gradients. *Curr Opin Cell Biol* 24, 245–253.

Johnson JM, Jin M, Lew DJ (2011). Symmetry breaking and the establishment of cell polarity in budding yeast. *Curr Opin Genet Dev* 21, 740–746.

Kasai H, Fukuda M, Watanabe S, Hayashi-Takagi A, Noguchi J (2010). Structural dynamics of dendritic spines in memory and cognition. *Trends Neurosci* 33, 121–129.

Keener JP (1986). A geometrical theory for spiral waves in excitable media. *SIAM J Appl Math* 46, 1039–1056.

Kim IH, Wang H, Soderling SH, Yasuda R (2014). Loss of Cdc42 leads to defects in synaptic plasticity and remote memory recall. *Elife* 3, 10.7554/eLife.02839.

Klunder B, Freisinger T, Wedlich-Soldner R, Frey E (2013). GDI-mediated cell polarization in yeast provides precise spatial and temporal control of Cdc42 signaling. *PLoS Comput Biol* 9, e1003396.

Kozubowski L, Saito K, Johnson JM, Howell AS, Zyla TR, Lew DJ (2008). Symmetry-breaking polarization driven by a Cdc42p GEF-PAK complex. *Curr Biol* 18, 1719–1726.

Kusters R, Kapitein LC, Hoogenraad CC, Storm C (2013). Shape-induced asymmetric diffusion in dendritic spines allows efficient synaptic AMPA receptor trapping. *Biophys J* 105, 2743–2750.

Lamprecht R, LeDoux J (2004). Structural plasticity and memory. *Nat Rev Neurosci* 5, 45–54.

Lommerse PH, Blab GA, Cognet L, Harms GS, Snaar-Jagalska BE, Spaink HP, Schmidt T (2004). Single-molecule imaging of the H-ras membrane-anchor reveals domains in the cytoplasmic leaflet of the cell membrane. *Biophys J* 86, 609–616.

Luo L (2002). Actin cytoskeleton regulation in neuronal morphogenesis and structural plasticity. *Annu Rev Cell Dev Biol* 18, 601–635.

Maletic-Savatic M, Malinow R, Svoboda K (1999). Rapid dendritic morphogenesis in CA1 hippocampal dendrites induced by synaptic activity. *Science* 283, 1923–1927.

Maree AF, Grieneisen VA, Edelstein-Keshet L (2012). How cells integrate complex stimuli: The effect of feedback from phosphoinositides and cell shape on cell polarization and motility. *PLoS Comput Biol* 8, e1002402.

Matsuzaki M, Honkura N, Ellis-Davies GC, Kasai H (2004). Structural basis of long-term potentiation in single dendritic spines. *Nature* 429, 761–766.

Mattila PK, Lappalainen P (2008). Filopodia: molecular architecture and cellular functions. *Nat Rev Mol Cell Biol* 9, 446–454.

Meyers J, Craig J, Odde DJ (2006). Potential for control of signaling pathways via cell size and shape. *Curr Biol* 16, 1685–1693.

- Michaud EJ, Yoder BK (2006). The primary cilium in cell signaling and cancer. *Cancer Res* 66, 6463–6467.
- Mori Y, Jilkine A, Edelstein-Keshet L (2008). Wave-pinning and cell polarity from a bistable reaction-diffusion system. *Biophys J* 94, 3684–3697.
- Murakoshi H, Iino R, Kobayashi T, Fujiwara T, Ohshima C, Yoshimura A, Kusumi A (2004). Single-molecule imaging analysis of ras activation in living cells. *Proc Natl Acad Sci USA* 101, 7317–7322.
- Murakoshi H, Wang H, Yasuda R (2011). Local, persistent activation of rho GTPases during plasticity of single dendritic spines. *Nature* 472, 100–104.
- Neves SR, Tsokas P, Sarkar A, Grace EA, Rangamani P, Taubenfeld SM, Alberini CM, Schaff JC, Blitzler RD, Moraru II, et al. (2008). Cell shape and negative links in regulatory motifs together control spatial information flow in signaling networks. *Cell* 133, 666–680.
- Noguchi J, Matsuzaki M, Ellis-Davies GCR, Kasai H (2005). Spine-neck geometry determines NMDA receptor-dependent Ca²⁺ signaling in dendrites. *Neuron* 46, 609–622.
- Rangamani P, Lipshtat A, Azeloglu EU, Calizo RC, Hu M, Ghassemi S, Hone J, Scarlata S, Neves SR, Iyengar R (2013). Decoding information in cell shape. *Cell* 154, 1356–1369.
- Schmick M, Bastiaens PI (2014). The interdependence of membrane shape and cellular signal processing. *Cell* 156, 1132–1138.
- Shin EY, Shin KS, Lee CS, Woo KN, Quan SH, Soung NK, Kim YG, Cha CI, Kim SR, Park D, et al. (2002). Phosphorylation of p85 beta PIX, a rac/Cdc42-specific guanine nucleotide exchange factor, via the ras/ERK/PAK2 pathway is required for basic fibroblast growth factor-induced neurite outgrowth. *J Biol Chem* 277, 44417–44430.
- Singla V, Reiter JF (2006). The primary cilium as the cell's antenna: signaling at a sensory organelle. *Science* 313, 629–633.
- Tilney LG, Tilney MS, Guild GM (1995). F actin bundles in drosophila bristles. I. Two filament cross-links are involved in bundling. *J Cell Biol* 130, 629–638.
- Tolias KF, Duman JG, Um K (2011). Control of synapse development and plasticity by rho GTPase regulatory proteins. *Prog Neurobiol* 94, 133–148.
- Tonnesen J, Katona G, Rozsa B, Nagerl UV (2014). Spine neck plasticity regulates compartmentalization of synapses. *Nat Neurosci* 17, 678–685.
- Tyson JJ, Keener JP (1988). Singular perturbation theory of traveling waves in excitable media (a review). *Physica D* 32, 327–361.
- Tyson JJ, Murray JD (1989). Cyclic AMP waves during aggregation of dictyostelium amoebae. *Development* 106, 421–426.
- Yasuda R, Murakoshi H (2011). The mechanisms underlying the spatial spreading of signaling activity. *Curr Opin Neurobiol* 21, 313–321.
- Yuste R, Bonhoeffer T (2004). Genesis of dendritic spines: Insights from ultrastructural and imaging studies. *Nat Rev Neurosci* 5, 24–34.
- Zykov VS (1980). Analytical evaluation of the dependence of the speed of an excitation wave in a two-dimensional excitable medium on the curvature of its front. *Biophysics* 25, 906–911.
- Zykov VS (1987). *Simulation of Wave Processes in Excitable Media*, Manchester, United Kingdom: Manchester University Press.